BBA - Molecular Basis of Disease 1869 (2023) 166818

Contents lists available at ScienceDirect

BBA - Molecular Basis of Disease

journal homepage: www.elsevier.com/locate/bbadis

Functional characterisation of the ACE2 orthologues in *Drosophila* provides insights into the neuromuscular complications of COVID-19

Paul Herrera, Ruben J. Cauchi *

Centre for Molecular Medicine and Biobanking, Biomedical Sciences Building, University of Malta, Msida, Malta
Department of Physiology and Biochemistry, Faculty of Medicine and Surgery, University of Malta, Msida, Malta

ARTICLE INFO

Keywords:
SARS-CoV-2
COVID-19
Drosophila
Ance
Ance-3
ACE2

ABSTRACT

SARS-CoV-2, the virus responsible for the coronavirus disease of 2019 (COVID-19), gains cellular entry *via* interaction with the angiotensin-converting enzyme 2 (ACE2) receptor of host cells. Although SARS-CoV-2 mainly targets the respiratory system, the neuromuscular system also appears to be affected in a large percentage of patients with acute or chronic COVID-19. The cause of the well-described neuromuscular manifestations resulting from SARS-CoV-2 infection remains unresolved. These may result from the neuromuscular-invasive capacity of the virus leading to direct injury. Alternatively, they may be the consequence of ACE2 inactivation either due to viral infection, ACE2 autoantibodies or both. Here, we made use of the *Drosophila* model to investigate whether ACE2 downregulation is sufficient to induce neuromuscular phenotypes. We show that moderate gene silencing of *ACE2* orthologues *Ance* or *Ance3* diminished survival on exposure to thermal stress only upon induction of neuromuscular fatigue driven by increased physical activity. A strong knockdown of *Ance* or *Ance3* directed to muscle reduced or abolished adult viability and caused obvious motoric deficits including reduced locomotion and impaired flight capacity. Selective knockdown of *Ance* and *Ance3* in neurons caused wing defects and an age-dependent decline in motor behaviour, respectively, in adult flies. Interestingly, RNA sequencing allowed us to discover several differentially spliced genes that are required for synaptic function downstream of *Ance* or *Ance3* depletion. Our findings are therefore supportive of the notion that loss of a RAS-independent function for ACE2 contributes to the neuromuscular manifestations associated with SARS-CoV-2 infection.

1. Introduction

The respiratory system is the major target of the severe acute respiratory syndrome coronavirus 2 (SARS-CoV-2), responsible for the coronavirus infectious disease of 2019 (COVID-19) pandemic [1]. However, based on numerous reports, the neuromuscular system appears to be affected in a large percentage of patients with an acute infection where common presentations include anosmia, dysgeusia, headache, dizziness, myalgia and myelitis [2–5]. Neuromuscular complications are more common in patients with chronic post-COVID syndrome, popularly known as 'long COVID'. Brain fog, muscle weakness and fatigue, exercise intolerance, and sensory disturbances, in addition to symptoms of autonomic dysfunction, have been reported in long COVID patients [6]. Viral infections can involve the neuromuscular system by differing mechanisms [7]. Viruses can be the direct cause of neuromuscular deficits as exemplified by Bell's palsy, a lower motor neuron-type unilateral facial weakness caused by reactivated herpesviruses including herpes simplex virus-1 or 2 and varicella zoster virus [8]. Alternatively, autoimmunity triggered by viral infection can give rise to neuromuscular disease as has recently been implicated for Epstein-Barr virus and Multiple Sclerosis, a demyelinating disease of the central nervous system [9,10]. Furthermore, viral exposures form part of the multifactorial aetiology of several chronic neuromuscular degenerative disorders including amyotrophic lateral sclerosis (ALS), a progressive

Abbreviations: A3SS, alternative 3′ splicing site; ACE2, angiotensin-converting enzyme 2; ALS, amyotrophic lateral sclerosis; COVID-19, coronavirus infectious disease of 2019; Dcr-2, Dicer-2; DEGs, differentially expressed genes; DSGs, differentially spliced genes; GO, Gene Ontology; L3, third instar; MXE, mutually exclusive exons; qRT-PCR, quantitative reverse transcription-polymerase chain reaction; RAS, renin-angiotensin system; RI, retained intron; SARS-CoV-2, severe acute respiratory syndrome coronavirus 2; SE, skipped exon; A5SS, alternative 5′ splicing site.

* Corresponding author.
E-mail address: ruben.cauchi@um.edu.mt (R.J. Cauchi).

https://doi.org/10.1016/j.bbadis.2023.166818
Received 14 March 2023; Received in revised form 26 June 2023; Accepted 21 July 2023
Available online 24 July 2023

motor neuron degenerative disease of mid-age [11].

SARS-CoV-2 gains cellular entry *via* interaction of the Spike (S) glycoprotein on its envelope with the angiotensin-converting enzyme 2 (ACE2) receptor of host cells [12]. ACE2 is expressed in both neurons and skeletal muscles [13–15], which supports infection susceptibility and direct injury by SARS-CoV-2 in both cell types. Virus-like particles, SARS-CoV-2 viral proteins and/or RNA in skeletal muscles and neurons were therefore detected in COVID-19 patients following post-mortem analysis [16–18]. SARS-CoV-2 infection also downregulates ACE2 expression [19] and this can potentially disrupt the operation of the renin-angiotensin system (RAS) or other, as yet unknown, functions of ACE2 in the neuromuscular system. Dysregulated RAS has been linked to deleterious consequences including skeletal muscle atrophy and neurodegeneration [20,21]. As an alternative or potentially overlapping mechanism, the activity of ACE2 can also be dampened by autoantibodies, which have been detected in patients with a history of SARS-CoV-2 infection [22]. ACE2 has been highly conserved throughout evolution, hence homologues or orthologues exist in several mammalian, invertebrate and bacterial species [23]. Model organisms therefore offer opportunities to investigate the probable cause of the neuromuscular complications in COVID-19. Particularly, the utility of *Drosophila* as a powerful model system to study virus-host interactions and pathogenicity of SARS-CoV-2 in addition to treatment identification against COVID-19 has been well demonstrated [24–27]. Furthermore, *Drosophila* has an advantage over other model systems considering that RAS substrates are not conserved [27], and this therefore allows the investigation of RAS-independent functions for ACE2 homologues in neurons and muscle in addition to determining whether their disruption can lead to phenotypes similar to those experienced by COVID-19 patients.

Drosophila is often the perfect choice of model organism for neuromuscular disease modelling based on several reasons including a short lifespan, a rich genetic toolbox, and a significant degree of molecular pathway conservation [28,29]. Flies can respond rapidly to stimulation as well as performing complex motoric behaviours because they have a sophisticated neuromuscular system that, though simpler relative to humans, has the basic sensory-motor circuitry, glia and multinucleate muscle fibres [30]. Flies have therefore been particularly successful in modelling motor neuron disease including ALS and in gaining insights on the function of several ALS genes in the motor system [31]. Here we make use of *Drosophila* to investigate the function of the ACE2 orthologues Ance and Ance3 particularly asking whether they play a crucial role in the motor system *in vivo*.

Making use of gene-specific silencing, we show that RNAi transgenes that induce a strong knockdown of either *Ance* or *Ance3* throughout the whole organism led to lethality prior to flies reaching the adult stage indicating that both genes have essential functions during development. Moderate Ance or Ance3 deficiency had a minimal impact or no effect on baseline motoric activity but adult flies with increased neuromuscular fatigue, due to a history of higher physical activity, showed significantly reduced survival when exposed to thermal stress. Reduced levels of Ance or Ance3 specifically in muscle abolished or reduced adult viability in addition to inducing obvious motoric deficits. Selective knockdown of Ance and Ance3 in neurons caused wing defects and an age-dependent decline in motor behaviour, respectively, in adult flies. Finally, RNA sequencing of flies with a global reduction of Ance or Ance3 revealed a significant degree of overlap in altered gene expression. Transcriptome analysis nonetheless allowed us to identify unique pathways that were differentially dysregulated downstream of a depletion in either protein. Intriguingly, several genes that are required for synaptic function were found differentially spliced in response to either Ance or Ance3 knockdown. Our findings therefore support the notion that loss of a RAS-independent function for ACE2 contributes to the neuromuscular manifestations associated with SARS-CoV-2 infection. Additionally, our study underscores the utility of *Drosophila* as an *in vivo* model for discovering novel ACE2 functions and the implications of their disruption in COVID-19 patients.

2. Methods and materials

2.1. Fly culture and stocks

Flies were cultured on food consisting of sugar, corn meal, yeast and agar in plastic tubes at an incubation temperature of 25C under 12 h day/night cycles unless otherwise stated. The RNAi transgenic constructs *Ance-IR^{AC4}* (ID: 41219), *Ance3-IR^{AC5}* (ID: 100891) and *Ance3-IR^{AC6}* (ID: 101665) were obtained from the Vienna *Drosophila* Resource Centre, Austria [32]. The RNAi transgenic construct *Ance-IR^{AC12}* (ID: 8827R-1) was obtained from the *Drosophila* Genetic Resource Centre at the Kyoto Institute of Technology, Kyoto, Japan. The *Dcr-2* transgene (ID: 24651) and several GAL4 drivers including *Act5C*-GAL4 (ID: 4414), *elav*-GAL4 (ID: 458), *OK6*-GAL4 (ID: 64199), *Repo*-GAL4 (ID: 7415), *how*-GAL4 (ID: 1767) and *Mef2*-GAL4 (ID: 27390) were obtained from the Bloomington *Drosophila* Stock Centre (NIH P40OD018537) at Indiana University, USA. Drivers *G14*-GAL4 (Brian McCabe at Ecole Polytechnique Fédérale de Lausanne, Lausanne, Switzerland), *G7*-GAL4 (Aaron DiAntonio at Washington University School of Medicine, St. Louis, Missouri, USA), *MHC*-GAL4 (Frank Schnorrer at Developmental Biology Institute of Marseille, Aix-Marseille Université, Marseille, France) and *btl*-GAL4 (Sofia J. Araújo at University of Barcelona, Barcelona, Spain) were generous gifts. The combination of the various genetic tools was performed according to standard genetic crossing schemes.

2.2. Protein alignment

To determine % amino acid similarity and identity between human ACE2 (NP_068576.1) and its *Drosophila* orthologues Ance (NP_001285915.1) and Ance3 (NP_001033904.1), we utilised the DRSC Integrative Ortholog Prediction Tool (DIOPT, https://www.flyrnai.org/diopt). Alignment of the *Drosophila* proteins with their human counterpart was performed by Clustal Omega (EMBL-EBI).

2.3. Drosophila activity monitoring

Automated monitoring of *Drosophila* activity has been described in detail previously [33]. In brief, male flies were transferred to glass tubes containing 2 % grape agar at one end and a cotton plug at the other end. The tubes were then placed in a *Drosophila* activity monitor or DAM (TriKinetics Inc., Waltham, Massachusetts, USA) which was incubated at a temperature of 25C and a 12 h day/night cycle. Activity of flies was automatically recorded every 5 min for a duration of 24 h. Infrared detectors within the DAM registered activity as a count each time a fly crossed a beam.

2.4. Resilience to heat stress

Individual male flies were transferred to cotton-plugged tubes containing 2 % grape agar. The tubes were then incubated at a temperature of 33C and monitored over an 80 h period. Death was recorded every hour until all flies had died. Both experimental and control genotypes were of the same age and were incubated simultaneously.

2.5. Treatment to unforced physical activity

On eclosion ~20 male flies were transferred to plastic tubes with fly food having a standard height of 6 cm from the food base till the plug's end. This setup provided normal levels of physical activity since *Drosophila* exhibits negative geotaxis behaviour, hence climbing the wall of the tube to reach the plug's end and returning back to the bottom to feed. To increase levels of daily physical activity in as gentle a manner as possible, on eclosion, flies were housed in plastic tubes with fly food

having an increased height of 14 cm from the food base till the plug's end.

2.6. Adult viability

Adult viability was calculated as the percentage of the number of adult flies with the appropriate genotype divided by the expected number for the cross. When indicated, a temperature of 29 °C was utilised to amplify GAL4 activity.

2.7. Larval locomotor behaviour

Locomotor behaviour in third instar (L3) larvae was assessed at 72 h (L3a) and 96 h (L3b) after egg laying. Briefly, larvae of the appropriate genotype were first placed on a 0.7 % agar plate and allowed to acclimatise for 5 min. The number of forward body wall contractions exhibited by the organism in 30 s was subsequently counted. Each larva was assessed three times before an average was taken. A minimum of 15 larvae per genotype was assayed.

2.8. Climbing performance

Two empty polystyrene tubes were vertically joined by tape facing each other. Flies (15–20) were then transferred to the lower tube and allowed to acclimatise. To stimulate climbing, flies were gently tapped down to the bottom of the tube. The number of flies per group that climbed above the 8 cm mark in 10 s were then counted to determine the percentage climbing success rate. Four trials were performed for each group of flies and a minimum of four replicates were assayed per genotype.

2.9. Flight capacity

The Droso-Drome apparatus, consisting of a 1 L glass bottle divided into 4 sectors of 5 cm each, spanning a total height of 20 cm, was utilised for assessment of flight performance as described previously [34]. An alcohol-based sticky fluid was used to coat the Droso-Drome walls allowing flies to stick at different sectors on drop-off. Flies first underwent a 'warm-up' by inducing negative geotaxis in an empty tube for 3 times. Organisms were then gently dropped into the Droso-Drome to induce flight. The number of flies distributed in each sector was next counted, divided by the total number of flies dropped and multiplied by 100 to generate the % number of flies per sector. Fight ability correlates with the sector in which flies are distributed on landing, hence, fly percentages that are skewed towards the lower sectors of the Droso-Drome are indicative of reduced flight capacity. A minimum of four replicates were assayed per genotype.

2.10. RNA extraction

RNA was extracted from 12 to 15 L3b larvae of the desired genotype using the Qiagen RNeasy Plus Mini Kit (Qiagen, Hilden, Germany) following manufacturer's instructions. In brief, whole larvae were homogenized and lysed. Tissue lysates were then spun through genomic DNA eliminator spin columns to remove genomic DNA and RNeasy Mini spin columns were subsequently used to purify total RNA.

2.11. Quantitative RT-PCR

Quantification of *Ance* and *Ance3* expression levels was achieved by amplifying the corresponding cDNA using the SOLIScript 1-step Solis-Green kit (Solis Biodyne, Tartu, Estonia) following manufacturer's instructions. The primers were obtained from Integrated DNA Technologies (Leuven, Belgium) and were specific for *Ance* (forward: 5′ – TGGGCTATGCTGCTCTACCT – 3′; reverse: 5′ – GCTGGTAAAGCGGACGAATA – 3′), *Ance3* (forward: 5′ – CGGTATAAAGCCCCCAGTTT – 3′; reverse: 5′ – CGATAAATGTCGCATTGGTG – 3′) and housekeeping gene *Gem3* (forward: 5′ – GGCACCTGGACAGGTTAAGA – 3′; reverse: 5′ – CCCGGTGTACCGATAATGAC – 3′). The transcriptional levels were calculated by the 2–ΔΔCt (Ct, cycle of threshold) method. ΔΔCt = ΔCt of experimental group – mean ΔCt of control groups. ΔCt = Ct (gene of interest) − Ct (housekeeping).

2.12. RNA-seq and data analysis

RNA-seq libraries from RNA samples derived from female L3 larvae (3 biological replicates) were prepared and sequenced at the Beijing Genomics Institute, Denmark. Briefly, poly(A) mRNA was enriched using poly(T) oligo-attached magnetic beads. This was followed by fragmentation and subsequent first strand cDNA synthesis using random hexamer N6 primers and reverse transcriptase. Following end repair and adaptor ligation, cDNA fragments were PCR amplified and purified to generate single-stranded DNA circles in a final library. DNA nanoballs were finally generated by rolling circle replication, which underwent paired end sequencing (100 bp) on the BGI DNBseq platform.

Raw reads were filtered using SOAPnuke [35] and clean reads were mapped to the reference *Drosophila* genome using HISAT2 [36]. Transcript quantification was obtained using RSEM and normalized as fragments per kilobase of transcript per million mapped reads (FPKM) [37]. Differentially expressed genes (DEGs) were identified by the DESeq2 algorithm with *p*-values adjusted for multiple comparisons by the Benjamini and Hochberg procedure, and differential expression of the genes determined using a false discovery rate (FDR) cut off of <0.05 [38]. DEGs with a >2 fold change ($\log2FC > \pm1$) were selected. Differentially spliced genes (DSGs) were detected using rMATS [39] and five types of alternative splicing events including skipped exon (SE), alternative 5′ splicing site (A5SS), alternative 3′ splicing site (A3SS), mutually exclusive exons (MXE) and retained intron (RI) were defined. Gene Ontology (GO) biological pathway and cell component analysis on DSGs and upregulated or downregulated DEGs was carried out using ShinyGO [40].

2.13. Statistical analysis

Values are presented as means ± SEM unless otherwise indicated. The unpaired *t*-test was used to compare measures between 2 groups whereas two-way ANOVA, followed by Bonferroni's *post hoc* test, was used for multiple comparisons with control (GraphPad Prism v9.4.1). For adult viability analysis, the one sample *t*-test was used to determine whether the percentage mean was different from 100 %. Differences in survival between two groups was determined by the log-rank test. Differences were deemed statistically significant if $p < 0.05$.

3. Results

3.1. Knockdown of Drosophila ACE2 orthologues Ance and Ance3

Ance and Ance3 are two predicted orthologues of ACE2 in *Drosophila*. Compared to their human counterpart, Ance has an amino acid similarity and identity of 56 % and 36 %, respectively (71 % coverage) (Supplementary materials Fig. 1A). Comparably, Ance3 has 51 % similar and 32 % identical amino acid sequences (65 % coverage) to ACE2 (Supplementary materials Fig. 1B). We employed the *UAS/GAL4* system to express RNAi transgenes targeting either *Ance* and *Ance3* predicted mRNA transcripts. *Ance*-directed transgenes *Ance-IR*^{AC4} and *Ance-IR*^{AC12} target similar sequences in the 5′ coding region of the mRNA transcript (Fig. 1A). RNAi constructs designed to silence *Ance3* target either the exon 5 sequence (*Ance3-IR*^{AC5}) or the last exon and a part of the 3′ untranslated region of the *Ance3* transcript (*Ance3-IR*^{AC6}) (Fig. 1B). To assess gene knockdown efficiency and specificity we then performed quantitative RT-PCR (qRT-PCR) on RNA extracted from L3 larvae with constitutive expression of each transgenic construct. We

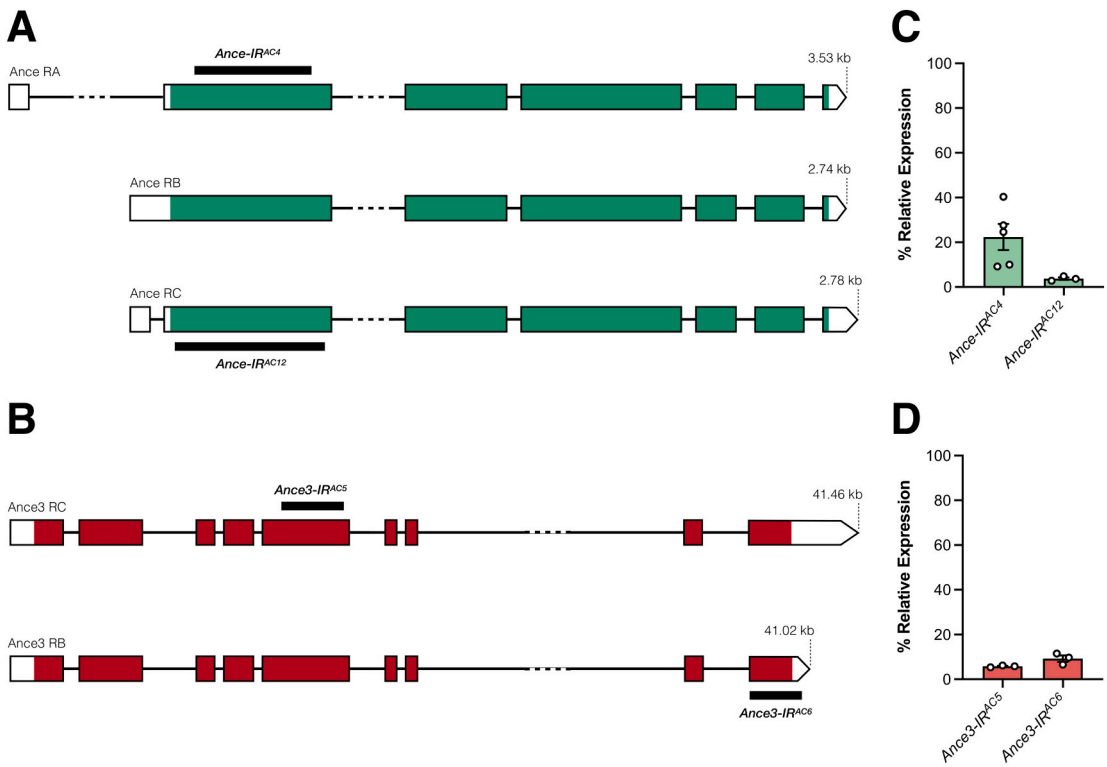

Fig. 1. Regions targeted by *Ance* or *Ance3* RNAi transgenes and residual expression on their activation. (**A**) Predicted *Ance* mRNA transcripts in *Drosophila* and regions targeted by RNAi constructs. Both *Ance-IR*^{AC4} and *Ance-IR*^{AC12} target similar sequences in the first exon of the *Ance* mRNA transcript. (**B**) Predicted *Ance3* mRNA transcripts and regions targeted by RNAi constructs. *Ance3-IR*^{AC5} targets exon 5 whereas *Ance3-IR*^{AC12} targets the last exon and a portion of the 3′ untranslated sequence of the *Ance3* mRNA transcript. (**C**) Expression of *Ance* relative to that of the housekeeping *Gem3* gene in L3b larvae in which the indicated RNAi transgene was constitutively expressed as determined by qRT-PCR. (**D**) *Ance3* expression levels relative to housekeeping *Gem3* gene in L3b larvae in which the indicated RNAi transgene was activated in the whole organism as determined by qRT-PCR. For **C** and **D**, each bar represents the mean ± SEM of at least three biological replicates with the respective data points superimposed on the bars.

show that activation of the *Ance-IR*^{AC4} construct induced a strong reduction in *Ance* transcript expression (22 %). A stronger knockdown of *Ance* was however achieved on constitutive activation of the *Ance-IR*^{AC12} transgene (4 %) (Fig. 1C). Turning to *Ance3*, we observed a robust knockdown for both *Ance3-IR*^{AC5} and *Ance3-IR*^{AC6} with the former leading to a stronger reduction in expression (6 %) compared to the latter (9 %) (Fig. 1D). Overall, these findings demonstrate that we have at hand RNAi constructs that target *Ance* and *Ance3* with specificity and differential efficiency, hence, allowing us to probe into the consequences of reduced protein levels *in vivo*.

3.2. Impact of Ance or Ance3 knockdown on baseline activity and stress resilience upon induction of neuromuscular fatigue

We discovered that, whereas constitutive *Ance-IR*^{AC12} expression induced lethality prior to adult development (puparial stage), flies in which *Ance-IR*^{AC4} was activated throughout the whole organism were adult viable. This difference in viability outcomes, which is likely related to the residual *Ance* expression levels in flies, gave us the opportunity to investigate the impact of moderate *Ance* knockdown on the baseline motoric ability of flies. To this end, we used a *Drosophila* Activity Monitor (DAM) to automatically track locomotion of individual flies during both day and night. A 24-hour activity profile shows that knockdown of *Ance* throughout the body in flies aged to day 15 post-eclosion caused an obvious decline in locomotor activity during day-time (Fig. 2A). On quantification, we noted a slight yet statistically significant drop in activity of flies with reduced levels of *Ance* compared to control flies during the day but not at night (Fig. 2B).

To uncover a covert motoric function that only becomes apparent upon induction of neuromuscular fatigue, we developed a protocol in which flies were treated to high levels of unforced physical activity post-eclosion and, then, tested the endurance of flies to a stressful condition. When 15 day-old flies with a history of normal physical activity were exposed to a temperature of 33C, we observed that flies with depleted levels of Ance had a similar survival decline as control flies (Fig. 2C). It is however noteworthy that gene silencing of *Ance* rendered flies that experienced high levels of physical activity remarkably less resilient to heat stress compared to control flies ($p = 0.0002$) (Fig. 2C). Hence, the median survival was reduced from 50 h in control flies to 46 h in flies having depletion of Ance, a substantial reduction of 4 h.

Turning to Ance3, we found that global activation of *Ance3-IR*^{AC5} led to pupal lethality where flies died as pharate adults that were not able to eclose from their pupal case. However, constitutive activation of the *Ance3-IR*^{AC6} transgene had no effect on adult fly viability, again, most probably the result of differences in knockdown efficiency. Reduced levels of Ance3 had no notable effect on baseline locomotor activity when monitoring flies for a 24 h period (Fig. 2D), hence, fly activity was not different from that of the control during both daytime and night-time (Fig. 2E). Nonetheless, similar to what we observed for *Ance*, knockdown of *Ance3* did not induce a significant decline in survival upon thermal exposure of flies with a history of normal physical activity. (Fig. 2F). However, a significant effect on survival was uncovered in flies that were exposed to higher levels of physical activity ($p = 0.0348$). Median survival was thus decreased by 11 h, from 35 h in the control to 46 h upon knockdown (Fig. 2F). In sum, these findings demonstrate that gene silencing of either *Ance* or *Ance3* had minimal or no impact on resting locomotor activity. However, in fatigued flies, reduced levels of either protein diminished resilience upon exposure to thermal stress with this hinting at a probable neuromuscular function for both Ance and Ance3.

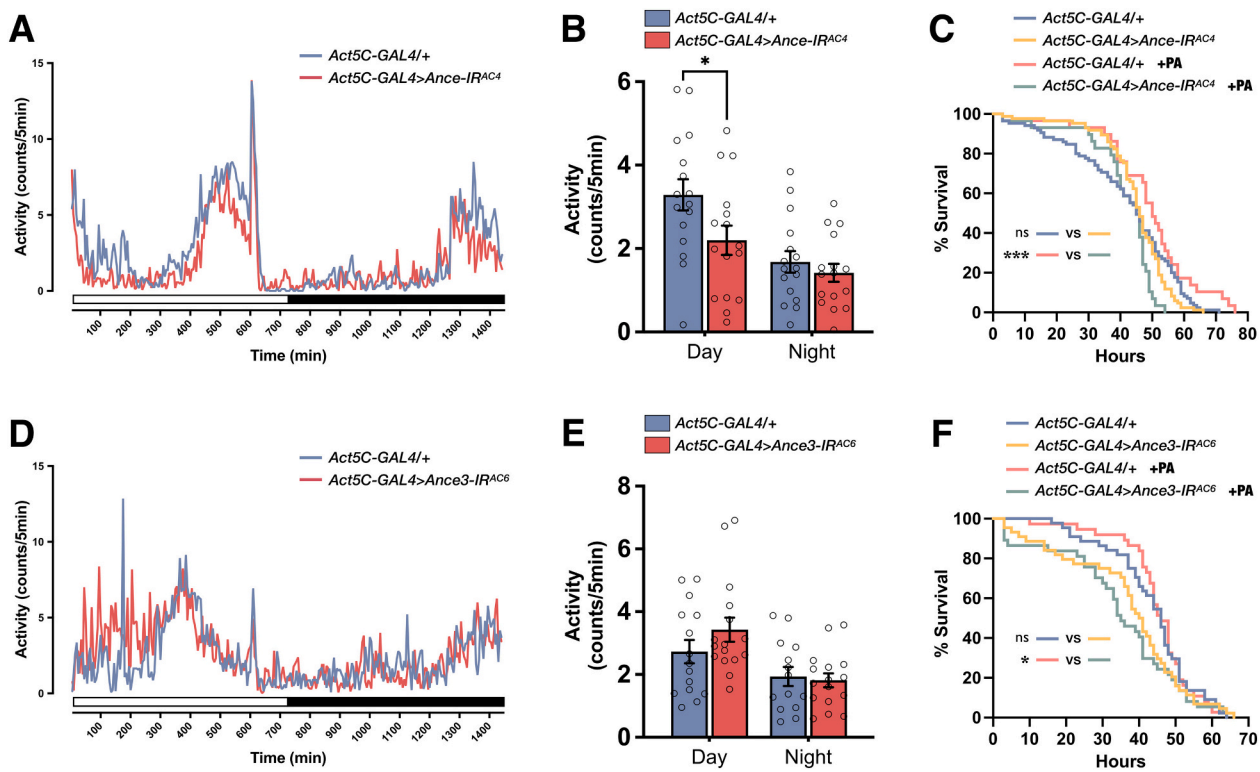

Fig. 2. Effect of constitutive knockdown of *Ance* or *Ance3* on baseline motoric activity and resilience to stress upon induction of neuromuscular fatigue driven by physical activity. (**A**) 24-hour activity profile of flies at day 15 post-eclosion. A decline in activity was obvious during daytime in flies with reduced levels of Ance. (**B**) 24-hour total activity chart of day 15 old flies confirmed that *Ance* knockdown induced a slight but significant drop in locomotor activity during the day but not at night. (**C**) A shift of temperature, from 25C to 33C, induced a decline in survival in 15 day old Ance knockdown *flies* that was not significantly different to that observed in control flies. A negative effect on survival upon exposure to thermal stress was however apparent in day 15 old flies cultured in conditions that favoured unforced physical activity (PA). (**D**) 24-hour activity profile of flies with *Ance3* knockdown at day 15 post-eclosion showed no obvious differences in locomotor ability. (**E**) 24-hour total activity chart of day 15 old flies confirmed that Ance3 knockdown had no significant negative consequences on motoric ability. (**F**) Exposure to hyperthermia led to a decrease in survival in day 15 old flies with *Ance3* knockdown compared to control, only upon PA treatment. In **A** and **D**, white and black rectangles on the x-axis represent light and dark periods, respectively. Plotted data is the average of activity summed in 5 min bins. In **B** and **E**, each bar represents the mean ± SEM of several independent experiments superimposed on the bars. Significance was tested by two-way ANOVA with Bonferroni's *post hoc* test (*$p = 0.03$). In C and F, significance was tested by the log-rank test (*$p = 0.0348$, and ***$p = 0.0002$). For all data, $n = 35$–45/genotype.

3.3. Tissue-specific effect of Ance or Ance3 knockdown on adult viability

To confirm whether Ance or Ance3 have an essential function in the motor system, we explored their compartment-specific requirements. To this end, we made use of various GAL4 drivers to induce tissue-specific activation of the strong RNAi transgenes *Ance-IR*^{AC12} and *Ance3-IR*^{AC5}. In humans, ACE2 expression in the upper respiratory tract correlates with the viral tropism of SARS-CoV-2 [41], and remarkably, we first show that lethality attributed to constitutive knockdown of Ance could be replicated when knockdown was restricted to tracheae, the fly equivalent of the respiratory tract (Fig. 3A). Importantly, restricting knockdown to muscle tissue starting from early development *via* the *how*-GAL4, *MHC*-GAL4 or *Mef2*-GAL4 drivers also caused a significant decline in adult viability when flies were cultured at 25C. Similar results were obtained following specific RNAi activation in glia (*Repo*-GAL4). Making use of these drivers, lethality or a further reduction in adult viability was apparent when efficiency of knockdown was intensified by increasing Dicer-2 (Dcr-2) levels and/or culturing flies at 29C, a temperature known to induce maximal GAL4 activity (Fig. 3A). No significant impact on adult viability was observed when Ance levels were selectively depleted in neurons (*elav*-GAL4) or, more specifically, motor neurons (*OK6*-GAL4).

Turning to Ance3, we observed that muscle-restricted knockdown starting from early development *via* the *Mef2*-GAL4 driver could also recapitulate the lethality observed on global gene silencing (Fig. 3B). A similar effect could be noted when expression of *Ance3-IR*^{AC5} was driven by the *how*-GAL4 driver at a temperature associated with higher GAL4 levels. Interestingly, selective knockdown of Ance3 in neurons (*elav*-GAL4) boosted by extra levels of Dcr-2 further resulted in a significant drop in adult viability when flies were cultured at 29C (Fig. 3B). Nonetheless, we saw no negative effect on survival to adulthood upon specific silencing of Ance3 in motor neurons, glia or trachea. In sum, these findings show that Ance and Ance3 have an essential role in the motor system starting from early development. However, they appear to have differential requirements with regards to cell types that comprise the motor system.

3.4. Motor impairment in flies with muscle selective loss of Ance or Ance3 function

Given that both Ance or Ance3 are required in muscle tissue for adult viability, we next asked whether loss of function of either protein would lead to an observable impairment in motoric ability, which is a true indicator of muscle weakness. We first induced knockdown of either Ance or Ance3, specifically directed to muscle tissue (*Mef2*-GAL4). Focusing on L3 larvae, we determined that flies with muscle-restricted downregulation of Ance, but not Ance3, experienced a significant drop in the body wall contraction rate. This was apparent at both the early L3a (72 h after egg laying) and the late L3b (96 h after egg laying) wandering stage (Fig. 4A). We did not observe a further decline in locomotor ability at either stage upon Dcr-2-enhanced knockdown of Ance (Fig. 4B). Next, we questioned whether defects in motoric ability were

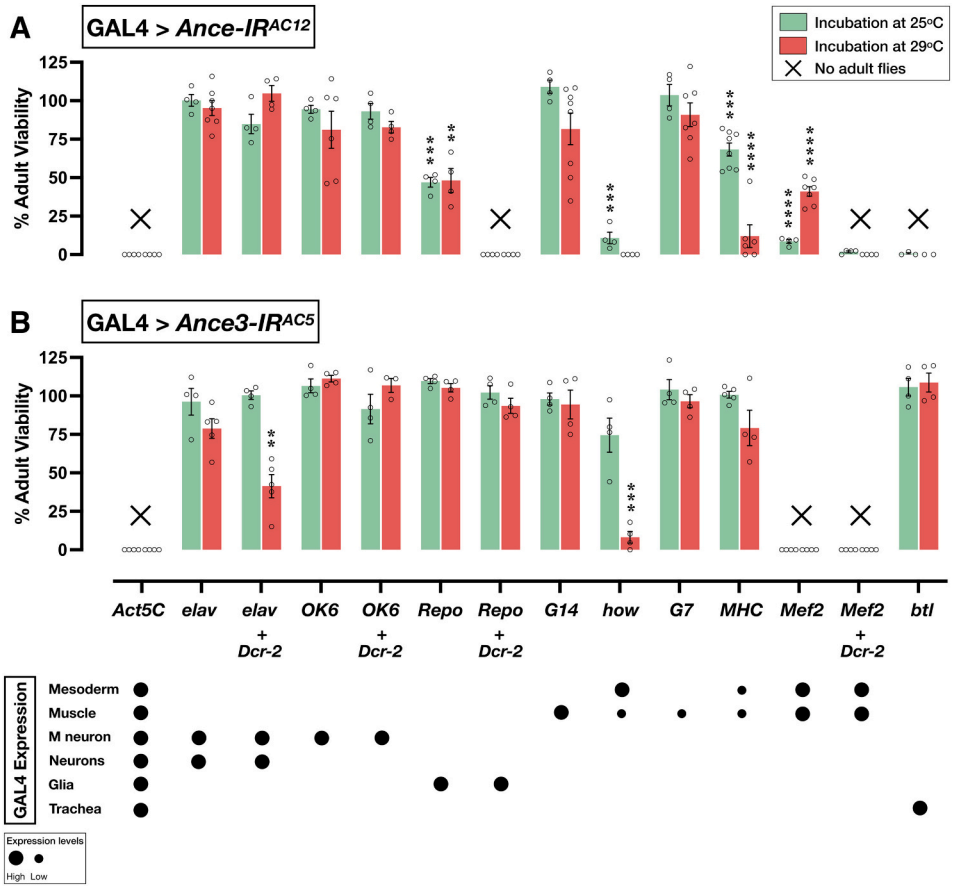

Fig. 3. Adult viability outcomes upon cell-type specific knockdown of *Ance* or *Ance3*. (**A**) Bar chart showing percentage adult viability on activation of *Ance-IR*^{AC12}, an RNAi transgene targeting *Ance*, in different cell types through the use of different GAL4 drivers. In view of lethality or a significant reduction in viability upon gene silencing, Ance is indispensable for adult viability in glia, muscle and airways. (**B**) Bar chart showing percentage adult viability on tissue-specific reduction of Ance3 expression brought about by activation of the *Ance3-IR*^{AC5} RNAi transgene. Ance3 is required in neurons and muscle for adult viability considering that a significant decline in viability or complete lethality was the outcome upon selective knockdown in the respective tissues. In **A** and **B**, individual bars represent the mean adult viability ± SEM normalized to the respective GAL4 driver control. Individual data points are superimposed on the bars. For each genotype, at least three independent experiments were conducted ($n \geq 100$ per genotype) and viability was assayed at a temperature of 25C and 29C. Where indicated, Dcr-2 was co-expressed to enhance knockdown. Significance, tested by the one sample *t*-test is indicated (**$p < 0.01$, ***$p < 0.001$, and ****$p < 0.0001$). Bottom panel shows expression patterns of the GAL4 driver lines.

obvious in adult flies with muscle-restricted Ance knockdown that escaped lethality. Indeed, when assessed at day 3 post-eclosion, we noticed that escapees had severe motoric deficits. Flight capacity was profoundly disrupted as observed by a significant percentage of flies that were distributed to the lowermost sector (sector 1) of the Droso-Drome apparatus (Fig. 4C). Flies with muscle-specific Ance deficiency also had severe mobility defects. Therefore, their climbing ability was also drastically reduced (Fig. 4D). Flies never lived beyond day 5 post-eclosion. These results prompted us to investigate whether similar phenotypes could be uncovered in adult flies with a muscle-restricted depletion in Ance3 levels. Interestingly, we also discovered severe flight impairments in flies in which the strong Ance3 RNAi transgene *Ance3-IR*^{AC5} was driven by the muscle-selective *MHC*-GAL4 driver (Fig. 4E). Relative to controls, flies also experienced significant deficits in climbing ability (Fig. 4F). Such behavioural alterations were observable in flies as early as day 5 post-eclosion. In summary, these findings support an important role for Ance or Ance3 in normal neuromuscular behaviour, specifically required in the muscle compartment of the motor system.

3.5. Neuron-selective downregulation of Ance3 affects motoric ability

Given the impact of muscle-restricted Ance or Ance3 deficiency on motoric behaviour, we wished to determine whether similar phenotypes can be observed for flies in which knockdown of Ance or Ance3 is selective to neurons. First, we observed that, although a reduction of Ance in neurons had no effect on adult fly viability, all eclosing flies showed an immature phenotype characterized by a failure to expand wings, cuticle defects including reduced sclerotization and melanisation, and disorganization of the scutellar bristles (Fig. 5A). This phenotype, which is a common encounter on disruption of several motor neuron disease linked genes [42–45], was however absent in flies with neuron-selective reduction in Ance3 levels. Nonetheless, we noticed that such flies developed climbing defects starting at day 15 post-eclosion (Fig. 5B). Furthermore, on assessment of flight performance we observed that a significant number of flies had flight defects as early as day 5 post-eclosion, which were found to subsequently worsen with age (Fig. 5C). Therefore, in addition to muscle, these findings also support a role for Ance or Ance3 in the neuronal compartment of the neuromuscular system.

3.6. Unique and overlapping transcriptional alterations in response to loss of Ance or Ance3

Finally, to identify the molecular changes responsible for the neuromuscular deficits we observed downstream of Ance or Ance3 loss of function, in addition to identifying overlapping alterations, we carried out RNA-sequencing (RNA-seq) in larvae with constitutive activation of the strong RNAi transgenes *Ance-IR*^{AC12} or *Ance3-IR*^{AC5}. We found 167 differentially expressed genes (DEGs) between *Ance* knockdown flies and control, of which 92 were downregulated and 75 were upregulated (Fig. 6A, Supplementary Materials Dataset S1). Only 3 downregulated transcripts were annotated as novel. When comparing Ance3 knockdown flies and control, we found 149 DEGs of which 88 were downregulated and 61 were upregulated (Fig. 6B, Supplementary Materials Dataset S2). In the *Ance3* dataset, 6 upregulated and 5 downregulated transcripts were annotated as novel.

It is interesting to note that several overlapping DEGs could be identified in the *Ance* and *Ance3* knockdown datasets, with changes in transcript levels mostly occurring in the same direction (Fig. 6C). Amongst the shared genes whose expression was increased upon either *Ance* or *Ance3* knockdown, half were ranked amongst the top 20

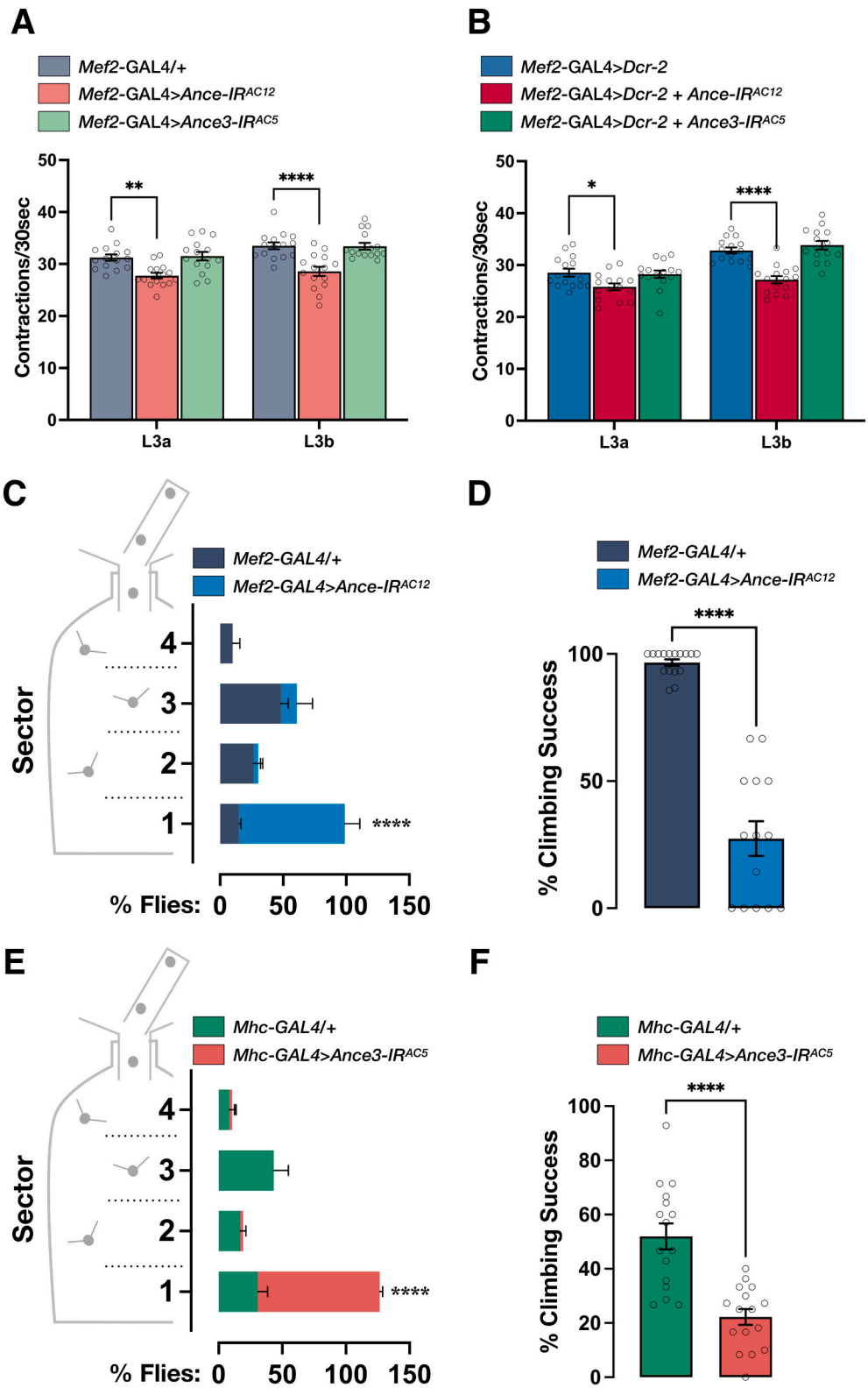

Fig. 4. Muscle-selective loss of Ance or Ance3 induces motor deficits. (**A**) Bar chart showing body wall contraction rate of L3 larvae with muscle-restricted downregulation of Ance or Ance3 assessed at 72 h (L3a) and, subsequently, 96 h (L3b) after egg laying (n = 15/genotype). A significant reduction is observed upon Ance but not Ance3 knockdown. (**B**) Bar chart showing body wall contraction rate of L3 larvae with muscle-restricted downregulation of Ance or Ance3 boosted by co-expression of Dcr-2. Behaviour was assessed at 72 h (L3a) and, subsequently, 96 h (L3b) after egg laying (n = 15/genotype). A significant reduction was observed upon *Ance*, but not *Ance3*, knockdown but the decline is not that different from that observed in flies without co-expression of Dcr-2. (**C**) Bar chart showing percentage distribution of flies landing in either of four sectors (4, top; 1, bottom) of the Droso-Drome apparatus after drop-off. Day 3-old adult flies with muscle-selective *Ance* knockdown had significant flight defects compared to the driver-only control ($n \geq 30$/genotype). (**D**) Bar chart showing that climbing ability was significantly impaired compared to the control in 3 day-old flies with muscle-restricted reduction of Ance ($n \geq 30$/genotype). (**E**) Bar chart showing percentage distribution of flies landing in each sector of the Droso-Drome apparatus after drop-off. When assessed at day 5 post-eclosion, flight capacity was impaired in adult flies with muscle-selective *Ance3* knockdown ($n \geq 60$/genotype). (**F**) Bar chart showing that Ance3 reduction in muscle also induced significant climbing defects in flies as early as day 5 post-eclosion ($n \geq 60$/genotype). In **A**–**F**, each bar represents the mean ± SEM of several independent experiments (superimposed on the bars in **A**, **B**, **D** and **F**). Significance was tested by two-way ANOVA with Bonferroni's *post hoc* test or the unpaired *t*-test and for all data, $^{*}p < 0.05$, $^{**}p < 0.01$, $^{***}p < 0.001$, and $^{****}p < 0.0001$.

upregulated DEGs in both datasets and included *Cyp6a2*, *Cyp4d14*, *CG30059*, *Cyp12d1-d*, *CG32214* and *CG42832* (Fig. 6A,B – genes annotated in red). However, only 15 % of the shared downregulated DEGs featured amongst the top 20 and included *CG10183*, *Ets21C*, *CG16775*, *CG8087*, and *CG32198* (Fig. 6A,B – genes annotated in blue). Intriguingly, we found the highest degree of overlap amongst the differentially spliced genes (DSGs) in response to knockdown of either *Ance* or *Ance3* (Fig. 6C). The overlaps in both DEGs and, particularly, DSGs were well above the overlap expected by random chance, with an estimated p value close to zero (upregulated DEGs, $p = 4.3 \times 10^{-16}$; downregulated DEGs, $p = 6.0 \times 10^{-49}$; DSGs, $p = 1.9 \times 10^{-54}$) according to the hypergeometric function for multi-set intersection analysis.

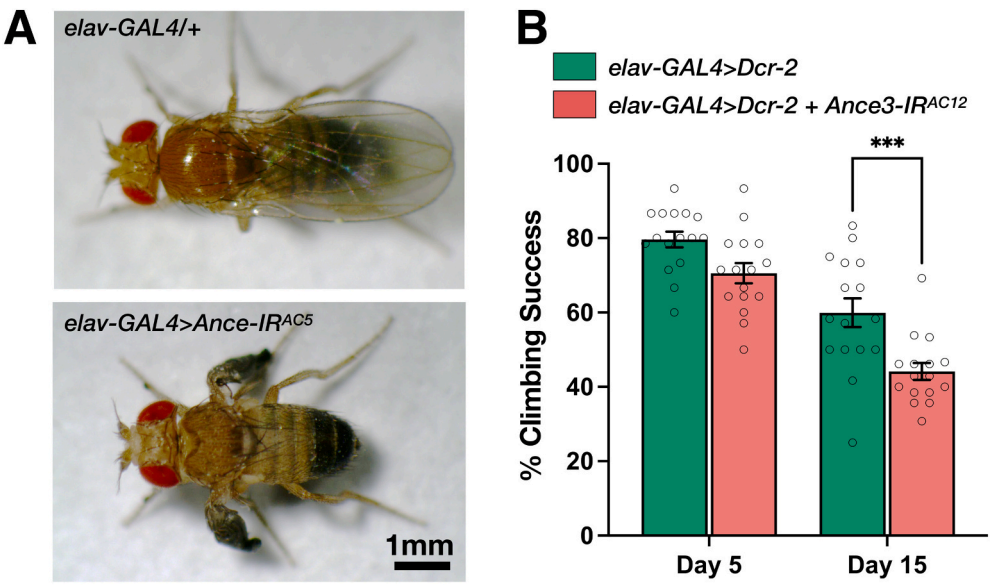

Fig. 5. Wing and motor deficits upon neuron-selective reduction of Ance or Ance3. (**A**) Representative images of a control fly (*upper panel*) and a fly with a neuronal reduction in Ance levels showing defects in cuticle hardening, tanning in addition to wing inflation (*lower panel*). (**B**) Bar chart showing that climbing ability is significantly impaired starting at day 15 post-eclosion in flies with brain-selective downregulation of Ance3 ($n \geq 60$/genotype). (**C**) Bar charts showing percentage number of organisms per sector for flies with neuron-selective Ance3 ablation assessed at two different timepoints throughout adulthood and compared to age-matched controls. Flight defects were apparent on day 5 post-eclosion and significantly worsened at day 15 post-eclosion ($n \geq 60$/genotype). In **B**–**C**, each bar represents the mean ± SEM of several independent experiments (superimposed on the bars in **B**). Significance was tested by two-way ANOVA with Bonferroni's *post hoc* test and for all data, $^{*}p < 0.05$, $^{***}p < 0.001$, and $^{****}p < 0.0001$.

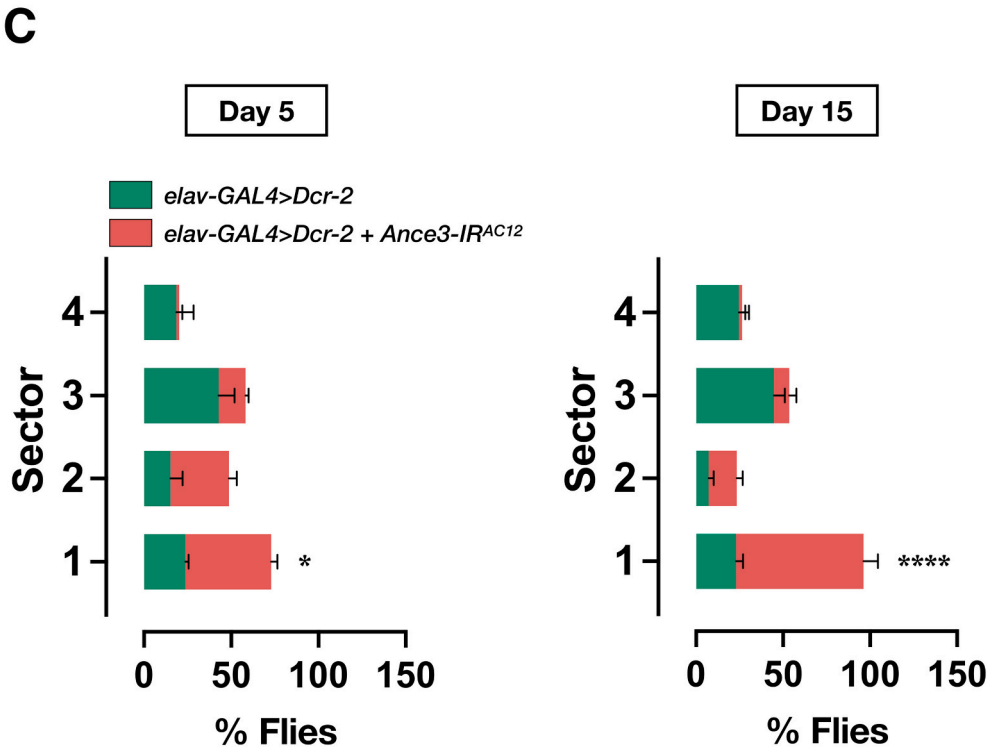

3.7. Pathway alterations in response to deficiency of Ance or Ance3

We next employed Gene Ontology (GO) enrichment analysis to identify dysregulated mechanisms downstream of Ance or Ance3 deficiency. GO biological pathway enrichment analysis on downregulated DEGs in response to knockdown of Ance revealed a significant inactivation of processes associated with immune defence and DNA repair (Fig. 7A). Applied to upregulated DEGs, GO biological pathway enrichment analysis identified a highly significant activation of processes associated with chromatin remodelling, in view of an increase in the expression of several histone genes (Fig. 7A). GO cellular component enrichment identified the nucleosome, particularly the protein-DNA packaging complex, as the cell structure mostly associated with upregulated DEGs (Fig. 7B). When applying GO biological pathway enrichment analysis on DEGs downstream of *Ance3* knockdown, we identified a downregulation of amino sugar breakdown (Fig. 7C). Metabolic processes that respond to toxin or insecticide uptake in addition to chaperone-mediated protein folding were however found to be upregulated (Fig. 7C). Construction of network plots shows a close association between the identified dysregulated biological pathways in response to *Ance* or *Ance3* ablation (Supplementary materials Fig. 2)

RNA-seq also revealed 97 differentially spliced genes (DSGs) upon *Ance* gene silencing, of which 20 had an alternative 3′ splice site (A3SS), 25 had an alternative 5′ splice site (A5SS), 11 had a mutually exclusive exon (MXE), 44 had a retained intron (RI) and 20 had a skipped exon (SE) (Supplementary materials Dataset S3). Several transcripts were subjected to more than one mode of alternative splicing (Supplementary materials Fig. 3A). Interestingly, although GO enrichment analysis on

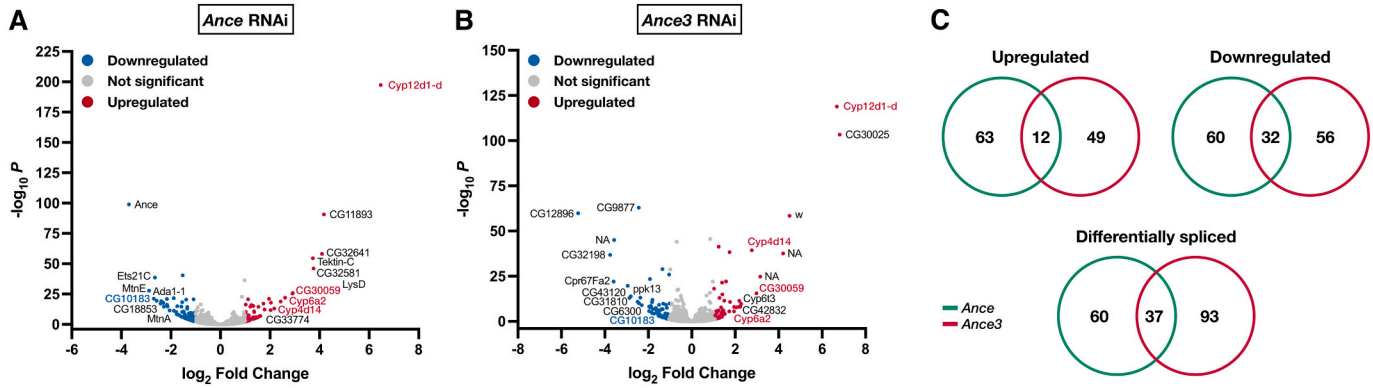

Fig. 6. Transcriptional alterations in response to constitutive *Ance* or *Ance3* gene silencing. (**A**) Volcano plot showing differentially expressed genes (DEGs) in L3b larvae with constitutive Ance knockdown compared to the driver-only control. Topmost significant DEGs have been annotated including those overlapping the Ance3 RNA-seq dataset (downregulated, blue; upregulated, red). (**B**) Volcano plot showing DEGs in L3b larvae with constitutive Ance3 knockdown compared to the driver-only control. Topmost significant DEGs have been annotated including those overlapping the Ance RNA-seq dataset (downregulated, blue; upregulated, red). (**C**) Venn diagrams showing number of unique and overlapping DEGs or DSGs in the Ance and Ance3 RNA-seq datasets.

DSGs revealed that cell-cell junction assembly and organisation was one of the top-most significantly enriched biological pathway terms, the process involving protein localization to the synapse was also found dysregulated (Fig. 8A). Corroborating these results, in addition to plasma membrane and cell junction, the synapse was amongst the topmost significantly enriched GO cell component terms (Fig. 8B). To this end, several proteins with a known function in synapse assembly, growth and/or function were all found to be subjected to several modes of alternative splicing (Table 1).

In flies with Ance3 knockdown, RNA-seq uncovered 130 differentially spliced genes (DSGs) with 21, 41, 23, 42 and 35 genes placed in the A3SS, A5SS, MXE, RI and SE alternative splicing category, respectively (Supplementary materials Dataset S4). Several transcripts were also subjected to more than one mode of alternative splicing (Supplementary materials Fig. 3B). DSG GO enrichment analysis showed that pathways involving actin filament organisation were amongst the top-most significantly enriched GO biological pathway terms. It is however noteworthy that synaptic signalling was also a significantly enriched GO term (Fig. 8C). Therefore, similar to what we observed for Ance, one of the topmost significantly enriched cell component terms downstream of Ance3 depletion was the synapse (Fig. 8D). Hence, several synaptic proteins, mostly different from those altered on Ance knockdown, were found alternatively spliced in response to Ance3 loss (Table 2). Overall, RNA-seq data revealed several transcriptome alterations that can explain the motor dysfunction resulting from loss of either Ance or Ance3 function.

4. Discussion

ACE2 is the indispensable entry receptor for multiple coronaviruses including SARS-CoV-2, responsible for a pandemic of unprecedented scale. Indeed, the COVID-19 pandemic has to date resulted in >675 million cases and 6.8 million deaths worldwide (Johns Hopkins University, 2023). The extraordinary intensive global effort to tackle SARS-CoV-2 has been translated into the most rapid development of vaccines and therapeutics, hence elevating ACE2 as one of the most researched proteins in such a short timeframe [41]. The cause of the extra-pulmonary manifestations resulting from SARS-CoV-2 infection, specifically those involving the neuromuscular system, remains unresolved. It is unclear whether the well-recorded neuromuscular symptoms observed in individuals with acute or chronic COVID-19 are the consequence of viral tropism, hence the targeting of extra-respiratory tissues, or else the result of autoimmunity-driven ACE2 inactivation. This prompted us to investigate whether ACE2 downregulation is sufficient to induce neuromuscular phenotypes. Making use of RNAi-mediated gene silencing in the *Drosophila* model system, we show that ACE2 orthologues Ance or Ance3 have a specific requirement in the motor system. Indeed, loss of their function increased neuromuscular fatigue inducing diminished survival upon stress exposure, and, importantly, it was enough to impair motoric ability. Amongst the identified transcriptional changes downstream of both Ance and Ance3 depletion, the greatest overlap was observed for genes that were differentially spliced with genes having a function in the synapse found to be particularly vulnerable to splicing alterations. Our findings are therefore supportive of a role for ACE2 downregulation as one of the triggers for the neuromuscular disturbances experienced by COVID-19 patients in addition to providing a plausible mechanism how this occurs.

We found that both *Ance* and *Ance3* are essential genes and, therefore, a severe global reduction in their transcript levels was found to induce lethality before the adult stage. This is a new discovery for *Ance3*, which has been relatively uncharacterised prior to our work. However, for *Ance*, our results are in contrast to those reported in the literature. Hence, although homozygous Ance mutations generated through chemical mutagenesis were found to experience a reduction in survival to adulthood [46], a recent study reported that Ance deletion resulted in flies that were completely adult viable [47]. This discrepancy could be due to the different techniques utilised or else the result of diverse genetic backgrounds, which can contain modifiers that allow survival to adulthood. The latter possibility has been observed for mouse *Ace2* knockout models [48]. Thus, in contrast to others but similar to our work, prenatal lethality was observed for *Ace2*$^{-/-}$ homozygous mutants as part of a systematic phenotypic mouse knockout project [49]. Studies like this including ours, therefore, question the redundancy of ACE2, its homologues or orthologues. RNA-seq data from the FlyAtlas 2 project show very high expression levels for Ance in the larval trachea, and high expression in the larval brain and muscles [50]. In line with this, our results show the highest disruption on survival to adulthood when *Ance* knockdown was restricted to trachea, glia, and muscle. This shows a good correlation between Ance's anatomical expression levels and its tissue-specific critical functions during development. For Ance3, FlyAtlas 2 data shows extremely low expression in the larval brain, and low expression in muscles [50]. In contrast, we report that muscle and, to a lesser extent, neurons, were the cell types that were mostly susceptible to reduced adult viability downstream of Ance3 depletion. These findings allow us to speculate that, for Ance3, expression levels are not a true indicator of its essential function in neuromuscular tissues during developmental progression.

We report that the downregulation of ACE2 orthologues in *Drosophila*, either within muscle or neurons, was enough to trigger motor dysfunction phenotypes similar to those observed in various fly

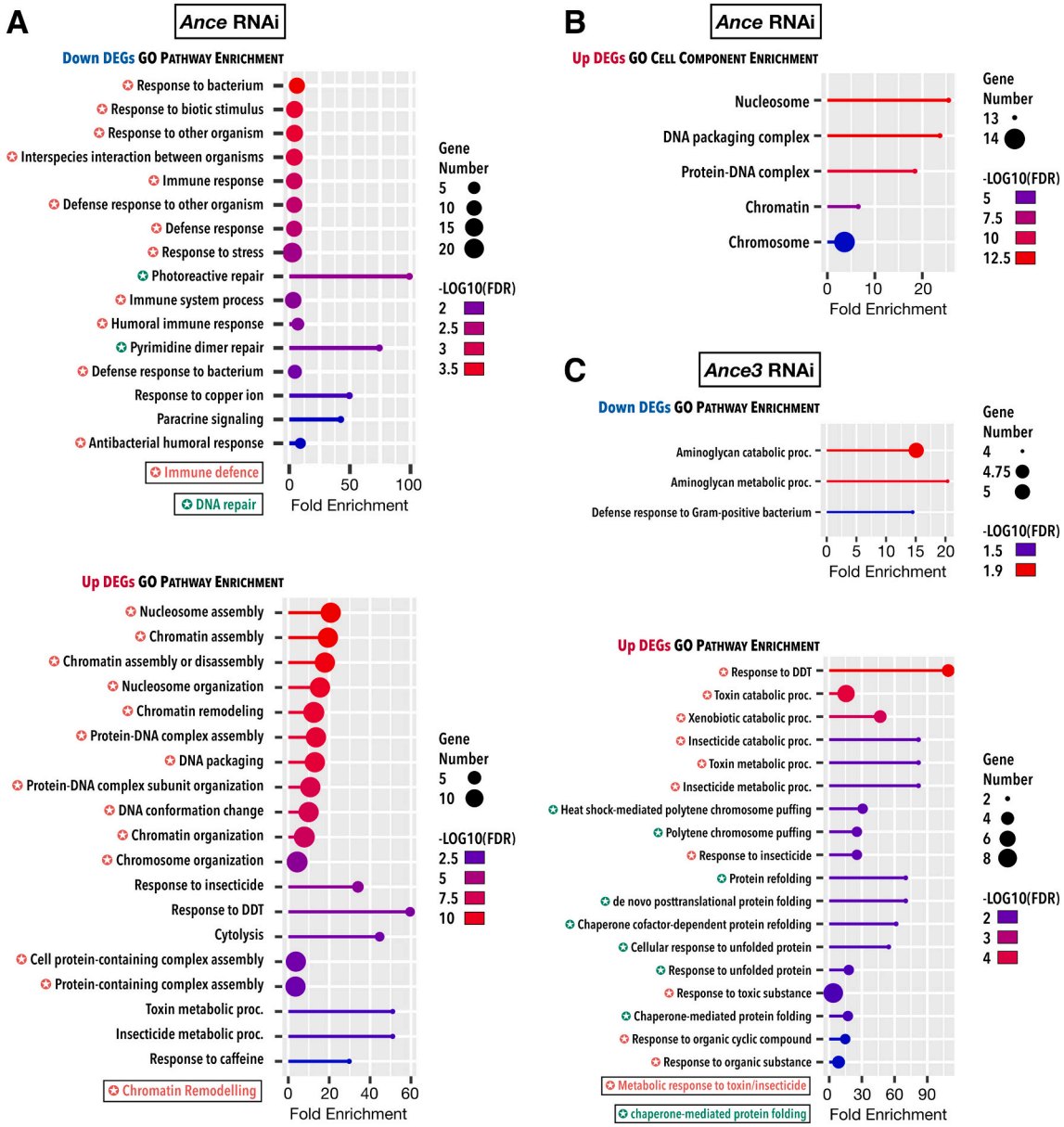

Fig. 7. Dysregulated pathways in response to Ance or Ance3 knockdown discovered through GO enrichment analysis of DEGs. (**A**) Lollipop plot presenting significant molecular pathway terms enriched in DEGs that were downregulated (upper panel) or upregulated (lower panel) in response to Ance knockdown. (**B**) Lollipop plot presenting significant cell component terms enriched in DEGs that were upregulated downstream of Ance deficiency. (**C**) Lollipop plot presenting significant molecular pathway terms enriched in DEGs that were downregulated (upper panel) or upregulated (lower panel) in response to Ance3 knockdown. In **A**–**C**, GO terms are sorted by FDR (<0.05) with the colour of the lollipops representing the values of the enrichment analysis relative to the other displayed terms (brighter red is more significant) and the size of the dots representing the number of genes that comprise the term. GO terms tagged with a colour-coded star indicate pathway overlap.

models of neuromuscular disease [28,30,31,34,51,52]. Our results are therefore supportive of the possibility that a dampened ACE2 function contributes to the neuromuscular manifestations of COVID-19. Diminished ACE2 function in COVID-19 patients could be the consequence of ACE2 autoantibodies [22]. ACE2 receptors expressed on muscle or neurons can also be saturated with viral particles and this could also potentially interfere with their function. The likelihood that COVID-19 neuromuscular disturbances are the direct result of injury caused by viral invasion still remains and is supported by several studies [16–18,53–56]. However, in other reports, SARS-CoV-2 viral proteins and/or RNA could not be detected in the cerebrospinal fluid, brain or skeletal muscle tissues of COVID-19 patients [57–61]. Studies that are supportive of a direct viral infection also suffer from criticisms including the probability that viral RNA is derived from blood vessels within samples or is the result of viral contamination [16,53]. Furthermore, when detected, the reported viral RNA levels were much lower than those observed in the nasal cavity [53]. Nonetheless, even if one still entertains the possibility of a direct viral invasion of the neuromuscular system, it is well known that SARS-CoV-2 can itself diminish ACE2 expression [19]. Considering the lack of conservation of RAS substrates in flies, our results point to loss of a RAS-independent function as the cause of the neuromuscular deficits, at least in the *Drosophila* model.

Transcriptome profiling revealed a significant degree of overlap in genes that are upregulated and downregulated in response to either Ance or Ance3 ablation. GO term gene enrichment analysis nonetheless pointed to different pathways that are disrupted downstream of a reduction in either protein. Hence, whereas immune defence, DNA repair and chromatin remodelling were the top dysregulated pathways following knockdown of Ance, gene silencing of Ance3 was found to perturb metabolic processes and chaperone-mediated protein folding.

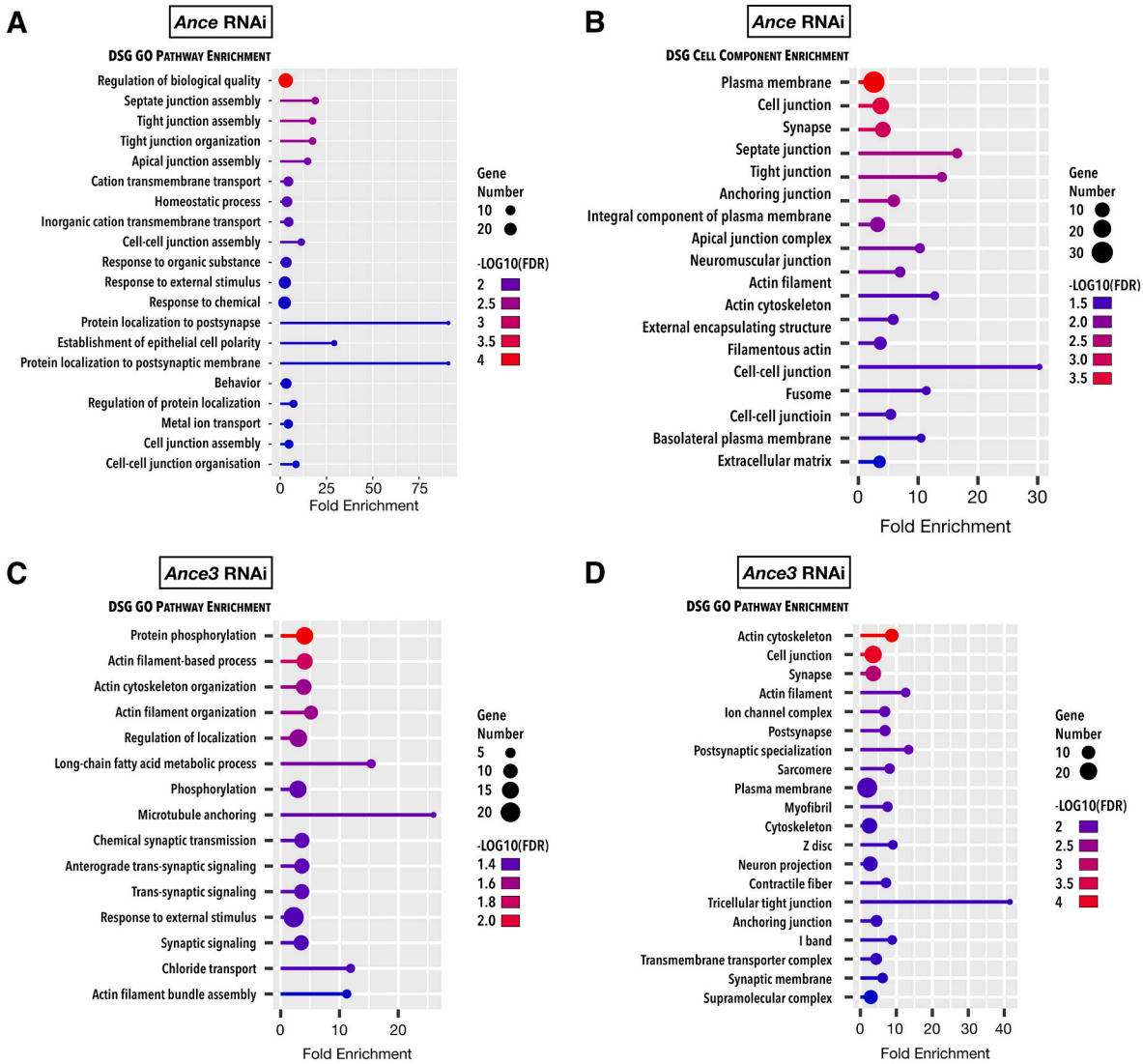

Fig. 8. GO enrichment analysis of DSGs identified dysregulated pathways downstream of Ance or Ance3 knockdown. (**A**) Lollipop plot showing the most significant GO molecular pathways terms enriched in DSGs identified in flies with Ance knockdown. (**B**) Lollipop plot showing the most significant GO cell component terms enriched in DSGs downstream of Ance knockdown. (**C**) Lollipop plot showing the most significant GO molecular pathway terms enriched in DSGs identified in flies with Ance3 knockdown. (**D**) Lollipop plot showing the most significant GO cell component terms enriched in DSGs downstream of Ance3 knockdown. In **A**–**D**, GO terms are sorted by FDR (<0.05) with the colour of the lollipops representing the values of the enrichment analysis relative to the other displayed terms (brighter red is more significant) and the size of the dots representing the number of genes that comprise the term.

However, it is notable that several genes involved in synapse function were found to be alternatively spliced, and this can help explain the motor behaviour deficits observed on loss of function of either of the two ACE2 *Drosophila* orthologues. It is still unclear how reduced levels of Ance or Ance3 leads to such consequential changes. Similar to ACE2, their human counterpart, Ance and Ance3 are predicted to act as metallopeptidases and, for Ance, this was experimentally confirmed [62,63]. Previous studies have shown a requirement for Ance during metamorphosis where it may process a developmental peptide hormone or, in concert with other peptidases, it may be involved in the recycling of larval protein amino acids for use in the synthesis of adult proteins [64]. The substrates catalysed by Ance or Ance3 remain unknown [27], therefore it is plausible that their incorrect processing is the trigger for the transcriptional alterations we observed in Ance and Ance3 knockdown flies.

The utility of *Drosophila* for understanding SARS-CoV-2 infection and the resulting disease manifestations has been solidified by various studies spurred by the global health emergency of the COVID-19 pandemic [25–27]. *Drosophila* has thus been exploited to investigate virus-host interactions and pathogenicity with studies demonstrating toxicity of various SARS-CoV-2 proteins [24,65]. Furthermore, a recent study which reported on the differential expression of *Drosophila* ACE2 orthologues in obesity, diabetes and aging models highlighted the use of the fly model in understanding the reasons why certain categories of individuals are more susceptible to COVID-19 severity [66]. The identification of chemicals that mitigate phenotypes linked to SARS-CoV-2 protein expression also shows the potential of flies as a powerful *in vivo* drug discovery platform [24,65]. Here, we add to these studies by showing that *Drosophila* can also be utilised to model the neuromuscular manifestations observed in COVID-19 patients. Importantly, our findings favour the possibility that these can partly arise from a down-regulation of ACE2. We also provide a mechanism by identifying several transcriptomic alterations expected to disrupt neuromuscular synaptic transmission upon loss of the ACE2 orthologues in *Drosophila*. Our study underscores *Drosophila* as a valuable *in vivo* model for understanding COVID-19 and cements its utility as a powerful tool in our arsenal in preparation for future coronavirus outbreaks.

Table 1
Genes with a synaptic function that are alternatively spliced downstream of *Ance* loss of function.

Gene	Protein	Alternative Splicing Events	Function
Atpalpha	Na pump α subunit	SE	An integral membrane cation antiporter protein that shuttles Na^+ and K^+ across the plasma membrane to maintain ion homeostasis and is required for synaptic assembly and transmission
Cirl	Calcium-independent receptor for α-latrotoxin	A5SS	G-protein coupled receptor required for adult locomotory behaviour
cv-c	crossveinless c	MXE, A5SS, RI	A RhoGTPase activating protein that regulates synaptic homeostasis at the NMJ
l(2)gl	lethal (2) giant larvae	SE	A tumour suppressor protein that regulates NMJ synapse morphology and function
Mical	Molecule interacting with CasL	MXE, RI, SE	A redox enzyme that regulates myofilament organisation and NMJ structure
nSyb	neuronal Synaptobrevin	A3SS	A SNARE involved in synaptic vesicle fusion and therefore required for synaptic signalling
Pak	p21-activated kinase	A5SS	A serine/threonine effector kinase that coordinates structural and functional synapse development at the NMJ
Sap47	Synapse-associated protein 47kD	RI	Protein that associates with synaptic vesicles and is required for intact synaptic and behavioural plasticity
scrib	scribble	A5SS	A scaffolding protein that regulates synaptic plasticity and synaptic vesicle dynamics
Sdc	Syndecan	A5SS, SE	A transmembrane heparan sulphate proteoglycan that promotes synapse growth at the larval NMJ
sgg	shaggy	RI	A glycogen synthase kinase required for synaptic assembly at the NMJ
sif	still life	A3SS	A guanine nucleotide exchange factor that localizes to presynaptic terminals and regulates synaptic growth of NMJs
unc-13	unc-13	SE, RI	A protein involved in synaptic vesicle exocytosis

Abbreviations: A3SS = alternative 3′ splice site; A5SS = alternative 5′ splice site; MXE = mutually exclusive exon; NMJ = neuromuscular junction; RI = retained intron; SE = skipped exon.

CRediT authorship contribution statement

Paul Herrera: Investigation, Methodology, Formal analysis, Data curation, Visualization, Writing – review & editing. **Ruben J. Cauchi:** Conceptualization, Methodology, Investigation, Formal analysis, Data curation, Writing – original draft, Writing – review & editing, Visualization, Supervision, Project administration, Funding acquisition.

Declaration of competing interest

The authors declare that they have no known competing financial interests or personal relationships that could have appeared to influence

Table 2
Genes with a synaptic function that are alternatively spliced downstream of *Ance3* loss of function.

Gene	Protein	Alternative Splicing Events	Function
Acsl	Acyl-CoA synthetase long-chain	A5SS	A protein with palmitoyl-CoA ligase activity that regulates axonal transport of synaptic vesicles and is required for synaptic development and transmission
Ank2	Ankyrin 2	SE	A cytoskeletal binding protein required for NMJ development and synaptic transmission
CaMKII	Calcium/calmodulin-dependent protein kinase II	A3SS, MXE, SE	A key regulator of plasticity in synaptic physiology and behaviour
CDase	Ceramidase	A5SS	A protein that regulates synaptic vesicle exocytosis and trafficking by controlling presynaptic terminal sphingolipid composition
CG1909	NA	A5SS, RI	A protein predicted to be involved in cholinergic synaptic transmission and positive regulation of neuromuscular synaptic transmission
eIF4E1	eukaryotic translation initiation factor 4E1	SE	A protein essential for cap-dependent translation of mRNA that plays a critical role in retrograde synaptic homeostasis at the NMJ
Gli	Gliotactin	A5SS	A transmembrane protein involved in synaptic target recognition
homer	Homer	A3SS	An adaptor protein that binds to group I metabotropic glutamate receptors, localizing to the synapse
l(2)gl	lethal (2) giant larvae	SE	A tumour suppressor protein that regulates NMJ synapse morphology and function
lap	like-AP180	MXE	A protein involved in clathrin-mediated endocytosis at the NMJ
Mical	Molecule interacting with CasL	MXE, SE	A redox enzyme that regulates myofilament organisation and NMJ structure
nAChRalpha5	nicotinic Acetylcholine Receptor α5	A5SS	A subunit of the nicotinic acetylcholine receptor involved in synaptic transmission
Pak	p21-activated kinase	A5SS	A serine/threonine effector kinase that coordinates structural and functional synapse development at the NMJ
pHCl-1	pH-sensitive chloride channel 1	MXE	A channel protein involved in chloride transmembrane transport predicted to be involved in synaptic transmission
Spn	Spinophilin	SE	A scaffold protein that regulates neurexin/neuroligin signalling at the presynaptic active zone

Abbreviations: A3SS = alternative 3′ splice site; A5SS = alternative 5′ splice site; MXE = mutually exclusive exon; NMJ = neuromuscular junction; RI = retained intron; SE = skipped exon.

the work reported in this paper.

Data availability

Data will be made available on request.

Acknowledgments

Dedicated with love to C.C. est. 2022. The authors are indebted to Matthew Camilleri for unwavering technical support. This work was supported by the Malta Council for Science & Technology COVID-19 R&D Fund (Project COV.RD.2020-22).

Appendix A. Supplementary data

Supplementary data to this article can be found online at https://doi.org/10.1016/j.bbadis.2023.166818.

References

[1] B. Hu, H. Guo, P. Zhou, Z.L. Shi, Characteristics of SARS-CoV-2 and COVID-19, Nat Rev Microbiol 19 (2021) 141–154.
[2] T. Shimohata, Neuro-COVID-19, Clin Exp Neuroimmunol 13 (2022) 17–23.
[3] C.C. Silva, C.N.C. Bichara, F.R.O. Carneiro, V. Palacios, A. Berg, J.A.S. Quaresma, L.F. Magno Falcao, Muscle dysfunction in the long coronavirus disease 2019 syndrome: pathogenesis and clinical approach, Rev. Med. Virol. 32 (2022), e2355.
[4] V.K. Paliwal, R.K. Garg, A. Gupta, N. Tejan, Neuromuscular presentations in patients with COVID-19, Neurol. Sci. 41 (2020) 3039–3056.
[5] J. Suh, A.A. Amato, Neuromuscular complications of coronavirus disease-19, Curr. Opin. Neurol. 34 (2021) 669–674.
[6] H.E. Davis, L. McCorkell, J.M. Vogel, E.J. Topol, Long COVID: major findings, mechanisms and recommendations, Nat Rev Microbiol 21 (2023) 133–146.
[7] S. Jacob, R. Kapadia, T. Soule, H. Luo, K.L. Schellenberg, R.N. Douville, G. Pfeffer, Neuromuscular complications of SARS-CoV-2 and other viral infections, Front. Neurol. 13 (2022), 914411.
[8] W. Zhang, L. Xu, T. Luo, F. Wu, B. Zhao, X. Li, The etiology of Bell's palsy: a review, J. Neurol. 267 (2020) 1896–1905.
[9] K. Bjornevik, M. Cortese, B.C. Healy, J. Kuhle, M.J. Mina, Y. Leng, S.J. Elledge, D. W. Niebuhr, A.I. Scher, K.L. Munger, A. Ascherio, Longitudinal analysis reveals high prevalence of Epstein-Barr virus associated with multiple sclerosis, Science 375 (2022) 296–301.
[10] T.V. Lanz, R.C. Brewer, P.P. Ho, J.S. Moon, K.M. Jude, D. Fernandez, R. A. Fernandes, A.M. Gomez, G.S. Nadj, C.M. Bartley, R.D. Schubert, I.A. Hawes, S. E. Vazquez, M. Iyer, J.B. Zuchero, B. Teegen, J.E. Dunn, C.B. Lock, L.B. Kipp, V. C. Cotham, B.M. Ueberheide, B.T. Aftab, M.S. Anderson, J.L. DeRisi, M.R. Wilson, R.J.M. Bashford-Rogers, M. Platten, K.C. Garcia, L. Steinman, W.H. Robinson, Clonally expanded B cells in multiple sclerosis bind EBV EBNA1 and GlialCAM, Nature 603 (2022) 321–327.
[11] T. Alfahad, A. Nath, Retroviruses and amyotrophic lateral sclerosis, Antivir. Res. 99 (2013) 180–187.
[12] M. Hoffmann, H. Kleine-Weber, S. Schroeder, N. Kruger, T. Herrler, S. Erichsen, T. S. Schiergens, G. Herrler, N.H. Wu, A. Nitsche, M.A. Muller, C. Drosten, S. Pohlmann, SARS-CoV-2 cell entry depends on ACE2 and TMPRSS2 and is blocked by a clinically proven protease inhibitor, Cell 181 (2020) 271–280 e278.
[13] M. Perez-Valera, M. Martinez-Canton, A. Gallego-Selles, V. Galvan-Alvarez, M. Gelabert-Rebato, D. Morales-Alamo, A. Santana, S. Martin-Rodriguez, J. G. Ponce-Gonzalez, S. Larsen, J. Losa-Reyna, I. Perez-Suarez, C. Dorado, D. Curtelin, J.J. Gonzalez-Henriquez, R. Boushel, J. Hallen, P. de Pablos Velasco, J. Freixinet-Gilart, H.C. Holmberg, J.W. Helge, M. Martin-Rincon, J.A.L., Calbet, angiotensin-converting enzyme 2 (SARS-CoV-2 receptor) expression in human skeletal muscle, Scand. J. Med. Sci. Sports 31 (2021) 2249–2258.
[14] R. Chen, K. Wang, J. Yu, D. Howard, L. French, Z. Chen, C. Wen, Z. Xu, The spatial and cell-type distribution of SARS-CoV-2 receptor ACE2 in the human and mouse brains, Front. Neurol. 11 (2020), 573095.
[15] M.Y. Li, L. Li, Y. Zhang, X.S. Wang, Expression of the SARS-CoV-2 cell receptor gene ACE2 in a wide variety of human tissues, Infect Dis Poverty 9 (2020) 45.
[16] A. Emmi, S. Rizzo, L. Barzon, M. Sandre, E. Carturan, A. Sinigaglia, S. Riccetti, M. Della Barbera, R. Boscolo-Berto, P. Cocco, V. Macchi, A. Antonini, M. De Gaspari, C. Basso, R. De Caro, A. Porzionato, Detection of SARS-CoV-2 viral proteins and genomic sequences in human brainstem nuclei, NPJ Parkinsons Dis 9 (2023) 25.
[17] J.E. Hooper, M. Uner, D.S. Priemer, A. Rosenberg, L. Chen, Muscle biopsy findings in a case of SARS-CoV-2-associated muscle injury, J. Neuropathol. Exp. Neurol. 80 (2021) 377–378.
[18] S.R. Stein, S.C. Ramelli, A. Grazioli, J.Y. Chung, M. Singh, C.K. Yinda, C.W. Winkler, J. Sun, J.M. Dickey, K. Ylaya, S.H. Ko, A.P. Platt, P.D. Burbelo, M. Quezado, S. Pittaluga, M. Purcell, V.J. Munster, F. Belinky, M.J. Ramos-Benitez, E. A. Boritz, I.A. Lach, D.L. Herr, J. Rabin, K.K. Saharia, R.J. Madathil, A. Tabatabai, S. Soherwardi, M.T. McCurdy, N.C.-A. Consortium, K.E. Peterson, J.I. Cohen, E. de Wit, K.M. Vannella, S.M. Hewitt, D.E. Kleiner, D.S. Chertow, SARS-CoV-2 infection and persistence in the human body and brain at autopsy, Nature 612 (2022) 758–763.
[19] Y. Lu, Q. Zhu, D.M. Fox, C. Gao, S.A. Stanley, K. Luo, SARS-CoV-2 down-regulates ACE2 through lysosomal degradation, Mol. Biol. Cell 33 (2022) ar147.
[20] C. Cabello-Verrugio, G. Cordova, J.D. Salas, Angiotensin II: role in skeletal muscle atrophy, Curr. Protein Pept. Sci. 13 (2012) 560–569.
[21] C. Cosardereliogl, L.S. Nidadavolu, C.J. George, E.S. Oh, D.A. Bennett, J. D. Walston, P.M. Abadir, Brain renin-angiotensin system at the intersect of physical and cognitive frailty, Front. Neurosci. 14 (2020), 586314.
[22] J.M. Arthur, J.C. Forrest, K.W. Boehme, J.L. Kennedy, S. Owens, C. Herzog, J. Liu, T.O. Harville, Development of ACE2 autoantibodies after SARS-CoV-2 infection, PLoS One 16 (2021), e0257016.
[23] L. Lubbe, G.E. Cozier, D. Oosthuizen, K.R. Acharya, E.D. Sturrock, ACE2 and ACE: structure-based insights into mechanism, regulation and receptor recognition by SARS-CoV, Clin Sci (Lond) 134 (2020) 2851–2871.
[24] J.Y. Zhu, J.G. Lee, J. van de Leemput, H. Lee, Z. Han, Functional analysis of SARS-CoV-2 proteins in Drosophila identifies Orf6-induced pathogenic effects with Selinexor as an effective treatment, Cell Biosci 11 (2021) 59.
[25] J. van de Leemput, Z. Han, Drosophila, a powerful model to study virus-host interactions and pathogenicity in the fight against SARS-CoV-2, Cell Biosci 11 (2021) 110.
[26] F. Nainu, D. Rahmatika, T.B. Emran, H. Harapan, Potential application of Drosophila melanogaster as a model organism in COVID-19-related research, Front. Pharmacol. 11 (2020), 588561.
[27] P. Herrera, R.J. Cauchi, ACE and ACE2: insights from Drosophila and implications for COVID-19, Heliyon 7 (2021), e08555.
[28] B. Aquilina, R.J. Cauchi, Modelling motor neuron disease in fruit flies: lessons from spinal muscular atrophy, J. Neurosci. Methods 310 (2018) 3–11.
[29] R.J. Cauchi, M. van den Heuvel, The fly as a model for neurodegenerative diseases: is it worth the jump? Neurodegener. Dis. 3 (2006) 338–356.
[30] T.E. Lloyd, J.P. Taylor, Flightless flies: Drosophila models of neuromuscular disease, Ann. N. Y. Acad. Sci. 1184 (2010) e1–20.
[31] F. Liguori, S. Amadio, C. Volonte, Fly for ALS: Drosophila modeling on the route to amyotrophic lateral sclerosis modifiers, Cell. Mol. Life Sci. 78 (2021) 6143–6160.
[32] G. Dietzl, D. Chen, F. Schnorrer, K.C. Su, Y. Barinova, M. Fellner, B. Gasser, K. Kinsey, S. Oppel, S. Scheiblauer, A. Couto, V. Marra, K. Keleman, B.J. Dickson, A genome-wide transgenic RNAi library for conditional gene inactivation in Drosophila, Nature 448 (2007) 151–156.
[33] J.C. Chiu, K.H. Low, D.H. Pike, E. Yildirim, I. Edery, Assaying locomotor activity to study circadian rhythms and sleep parameters in Drosophila, J. Vis. Exp. 43 (2010) 2157.
[34] R. Cacciottolo, J. Ciantar, M. Lanfranco, R.M. Borg, N. Vassallo, R. Bordonne, R. J. Cauchi, SMN complex member Gemin3 self-interacts and has a functional relationship with ALS-linked proteins TDP-43, FUS and Sod1, Sci. Rep. 9 (2019) 18666.
[35] R. Li, C. Yu, Y. Li, T.W. Lam, S.M. Yiu, K. Kristiansen, J. Wang, SOAP2: an improved ultrafast tool for short read alignment, Bioinformatics 25 (2009) 1966–1967.
[36] D. Kim, J.M. Paggi, C. Park, C. Bennett, S.L. Salzberg, Graph-based genome alignment and genotyping with HISAT2 and HISAT-genotype, Nat. Biotechnol. 37 (2019) 907–915.
[37] B. Li, C.N. Dewey, RSEM: accurate transcript quantification from RNA-Seq data with or without a reference genome, BMC Bioinformatics 12 (2011) 323.
[38] M.I. Love, W. Huber, S. Anders, Moderated estimation of fold change and dispersion for RNA-seq data with DESeq2, Genome Biol. 15 (2014) 550.
[39] S. Shen, J.W. Park, Z.X. Lu, L. Lin, M.D. Henry, Y.N. Wu, Q. Zhou, Y. Xing, rMATS: robust and flexible detection of differential alternative splicing from replicate RNA-Seq data, Proc. Natl. Acad. Sci. U. S. A. 111 (2014) E5593–E5601.
[40] S.X. Ge, D. Jung, R. Yao, ShinyGO: a graphical gene-set enrichment tool for animals and plants, Bioinformatics 36 (2020) 2628–2629.
[41] G.Y. Oudit, K. Wang, A. Viveiros, M.J. Kellner, J.M. Penninger, Angiotensin-converting enzyme 2-at the heart of the COVID-19 pandemic, Cell 186 (2023) 906–922.
[42] B.M. Woolums, B.A. McCray, H. Sung, M. Tabuchi, J.M. Sullivan, K.T. Ruppell, Y. Yang, C. Mamah, W.H. Aisenberg, P.C. Saavedra-Rivera, B.S. Larin, A.R. Lau, D. N. Robinson, Y. Xiang, M.N. Wu, C.J. Sumner, T.E. Lloyd, TRPV4 disrupts mitochondrial transport and causes axonal degeneration via a CaMKII-dependent elevation of intracellular Ca(2), Nat. Commun. 11 (2020) 2679.
[43] E. Storkebaum, R. Leitao-Goncalves, T. Godenschwege, L. Nangle, M. Mejia, I. Bosmans, T. Ooms, A. Jacobs, P. Van Dijck, X.L. Yang, P. Schimmel, K. Norga, V. Timmerman, P. Callaerts, A. Jordanova, Dominant mutations in the tyrosyl-tRNA synthetase gene recapitulate in Drosophila features of human Charcot-Marie-Tooth neuropathy, Proc. Natl. Acad. Sci. U. S. A. 106 (2009) 11782–11787.
[44] L. Vanden Broeck, M. Naval-Sanchez, Y. Adachi, D. Diaper, P. Dourlen, J. Chapuis, G. Kleinberger, M. Gistelinck, C. Van Broeckhoven, J.C. Lambert, F. Hirth, S. Aerts, P. Callaerts, B. Dermaut, TDP-43 loss-of-function causes neuronal loss due to defective steroid receptor-mediated gene program switching in Drosophila, Cell Rep. 3 (2013) 160–172.
[45] J. Steyaert, W. Scheveneels, J. Vanneste, P. Van Damme, W. Robberecht, P. Callaerts, E. Bogaert, L. Van Den Bosch, FUS-induced neurotoxicity in

Drosophila is prevented by downregulating nucleocytoplasmic transport proteins, Hum. Mol. Genet. 27 (2018) 4103–4116.
[46] D. Hurst, C.M. Rylett, R.E. Isaac, A.D. Shirras, The drosophila angiotensin-converting enzyme homologue Ance is required for spermiogenesis, Dev. Biol. 254 (2003) 238–247.
[47] A.R. Kim, E.B. Choi, M.Y. Kim, K.W. Choi, Angiotensin-converting enzyme Ance is cooperatively regulated by mad and pannier in Drosophila imaginal discs, Sci. Rep. 7 (2017) 13174.
[48] H. Jia, X. Yue, E. Lazartigues, ACE2 mouse models: a toolbox for cardiovascular and pulmonary research, Nat. Commun. 11 (2020) 5165.
[49] T. Tang, L. Li, J. Tang, Y. Li, W.Y. Lin, F. Martin, D. Grant, M. Solloway, L. Parker, W. Ye, W. Forrest, N. Ghilardi, T. Oravecz, K.A. Platt, D.S. Rice, G.M. Hansen, A. Abuin, D.E. Eberhart, P. Godowski, K.H. Holt, A. Peterson, B.P. Zambrowicz, F. J. de Sauvage, A mouse knockout library for secreted and transmembrane proteins, Nat. Biotechnol. 28 (2010) 749–755.
[50] D.P. Leader, S.A. Krause, A. Pandit, S.A. Davies, J.A.T. Dow, FlyAtlas 2: a new version of the Drosophila melanogaster expression atlas with RNA-Seq, miRNA-Seq and sex-specific data, Nucleic Acids Res. 46 (2018) D809–D815.
[51] L. McGurk, A. Berson, N.M. Bonini, Drosophila as an in vivo model for human neurodegenerative disease, Genetics 201 (2015) 377–402.
[52] R. Borg, A. Purkiss, R. Cacciottolo, P. Herrera, R.J. Cauchi, Loss of amyotrophic lateral sclerosis risk factor SCFD1 causes motor dysfunction in Drosophila, Neurobiol. Aging 126 (2023) 67–76.
[53] K.T. Thakur, E.H. Miller, M.D. Glendinning, O. Al-Dalahmah, M.A. Banu, A. K. Boehme, A.L. Boubour, S.S. Bruce, A.M. Chong, J. Claassen, P.L. Faust, G. Hargus, R.A. Hickman, S. Jambawalikar, A.G. Khandji, C.Y. Kim, R.S. Klein, A. Lignelli-Dipple, C.C. Lin, Y. Liu, M.L. Miller, G. Moonis, A.S. Nordvig, J. B. Overdevest, M.L. Prust, S. Przedborski, W.H. Roth, A. Soung, K. Tanji, A. F. Teich, D. Agalliu, A.C. Uhlemann, J.E. Goldman, P. Canoll, COVID-19 neuropathology at Columbia University Irving Medical Center/New York Presbyterian Hospital, Brain 144 (2021) 2696–2708.
[54] V.G. Puelles, M. Lutgehetmann, M.T. Lindenmeyer, J.P. Sperhake, M.N. Wong, L. Allweiss, S. Chilla, A. Heinemann, N. Wanner, S. Liu, F. Braun, S. Lu, S. Pfefferle, A.S. Schroder, C. Edler, O. Gross, M. Glatzel, D. Wichmann, T. Wiech, S. Kluge, K. Pueschel, M. Aepfelbacher, T.B. Huber, Multiorgan and renal tropism of SARS-CoV-2, N. Engl. J. Med. 383 (2020) 590–592.
[55] J. Matschke, M. Lutgehetmann, C. Hagel, J.P. Sperhake, A.S. Schroder, C. Edler, H. Mushumba, A. Fitzek, L. Allweiss, M. Dandri, M. Dottermusch, A. Heinemann, S. Pfefferle, M. Schwabenland, D. Sumner Magruder, S. Bonn, M. Prinz, C. Gerloff, K. Puschel, S. Krasemann, M. Aepfelbacher, M. Glatzel, Neuropathology of patients with COVID-19 in Germany: a post-mortem case series, Lancet Neurol. 19 (2020) 919–929.
[56] J. Meinhardt, J. Radke, C. Dittmayer, J. Franz, C. Thomas, R. Mothes, M. Laue, J. Schneider, S. Brunink, S. Greuel, M. Lehmann, O. Hassan, T. Aschman, E. Schumann, R.L. Chua, C. Conrad, R. Eils, W. Stenzel, M. Windgassen, L. Rossler, H.H. Goebel, H.R. Gelderblom, H. Martin, A. Nitsche, W.J. Schulz-Schaeffer, S. Hakroush, M.S. Winkler, B. Tampe, F. Scheibe, P. Kortvelyessy, D. Reinhold, B. Siegmund, A.A. Kuhl, S. Elezkurtaj, D. Horst, L. Oesterhelweg, M. Tsokos, B. Ingold-Heppner, C. Stadelmann, C. Drosten, V.M. Corman, H. Radbruch, F. L. Heppner, Olfactory transmucosal SARS-CoV-2 invasion as a port of central nervous system entry in individuals with COVID-19, Nat. Neurosci. 24 (2021) 168–175.
[57] T. Aschman, E. Wyler, O. Baum, A. Hentschel, F. Legler, C. Preusse, L. Meyer-Arndt, I. Büttnerova, A. Förster, D. Cengiz, L.G. Teixeira Alves, J. Schneider, C. Kedor, R. Rust, J. Bellmann-Strobl, S. Aminaa, P. Vajkoczy, H.-H. Goebel, M. Landthaler, V. Corman, A. Roos, F.L. Heppner, H. Radbruch, F. Paul, C. Scheibenbogen, W. Stenzel, N.F. Dengler, Post-COVID syndrome is associated with capillary alterations, macrophage infiltration and distinct transcriptomic signatures in skeletal muscles, medRxiv (2023), 2023.2002.2015.23285584.
[58] J. Helms, S. Kremer, H. Merdji, R. Clere-Jehl, M. Schenck, C. Kummerlen, O. Collange, C. Boulay, S. Fafi-Kremer, M. Ohana, M. Anheim, F. Meziani, Neurologic features in severe SARS-CoV-2 infection, N. Engl. J. Med. 382 (2020) 2268–2270.
[59] M. Schwabenland, H. Salie, J. Tanevski, S. Killmer, M.S. Lago, A.E. Schlaak, L. Mayer, J. Matschke, K. Puschel, A. Fitzek, B. Ondruschka, H.E. Mei, T. Boettler, C. Neumann-Haefelin, M. Hofmann, A. Breithaupt, N. Genc, C. Stadelmann, J. Saez-Rodriguez, P. Bronsert, K.P. Knobeloch, T. Blank, R. Thimme, M. Glatzel, M. Prinz, B. Bengsch, Deep spatial profiling of human COVID-19 brains reveals neuroinflammation with distinct microanatomical microglia-T-cell interactions, Immunity 54 (2021) 1594–1610 e1511.
[60] J.F. Fullard, H.C. Lee, G. Voloudakis, S. Suo, B. Javidfar, Z. Shao, C. Peter, W. Zhang, S. Jiang, A. Corvelo, H. Wargnier, E. Woodoff-Leith, D.P. Purohit, S. Ahuja, N.M. Tsankova, N. Jette, G.E. Hoffman, S. Akbarian, M. Fowkes, J. F. Crary, G.C. Yuan, P. Roussos, Single-nucleus transcriptome analysis of human brain immune response in patients with severe COVID-19, Genome Med 13 (2021) 118.
[61] I.H. Solomon, E. Normandin, S. Bhattacharyya, S.S. Mukerji, K. Keller, A.S. Ali, G. Adams, J.L. Hornick, R.F. Padera Jr., P. Sabeti, Neuropathological features of Covid-19, N. Engl. J. Med. 383 (2020) 989–992.
[62] M.J. Cornell, T.A. Williams, N.S. Lamango, D. Coates, P. Corvol, F. Soubrier, J. Hoheisel, H. Lehrach, R.E. Isaac, Cloning and expression of an evolutionary conserved single-domain angiotensin converting enzyme from Drosophila melanogaster, J. Biol. Chem. 270 (1995) 13613–13619.
[63] X. Houard, T.A. Williams, A. Michaud, P. Dani, R.E. Isaac, A.D. Shirras, D. Coates, P. Corvol, The *Drosophila melanogaster*-related angiotensin-I-converting enzymes Acer and Ance—distinct enzymic characteristics and alternative expression during pupal development, Eur. J. Biochem. 257 (1998) 599–606.
[64] R.J. Siviter, C.A. Taylor, D.M. Cottam, A. Denton, M.P. Dani, M.J. Milner, A. D. Shirras, R.E. Isaac, Ance, a Drosophila angiotensin-converting enzyme homologue, is expressed in imaginal cells during metamorphosis and is regulated by the steroid, 20-hydroxyecdysone, Biochem. J. 367 (2002) 187–193.
[65] S. Yang, M. Tian, A.N. Johnson, SARS-CoV-2 protein ORF3a is pathogenic in Drosophila and causes phenotypes associated with COVID-19 post-viral syndrome, bioRxiv (2020), 2020.12.20.423533.
[66] T. Duarte, M.M. Silva, P. Michelotti, N.B.V. Barbosa, B.C. Feltes, M. Dorn, J. Rocha, C.L. Dalla Corte, The Drosophila melanogaster ACE2 ortholog genes are differently expressed in obesity/diabetes and aging models: implications for COVID-19 pathology, Biochim. Biophys. Acta Mol. basis Dis. 1868 (2022), 166551.